Scientific Journal of King Faisal University:
Basic and Applied Sciences

Modified Efficient Net of Chest X-Ray Images for Lung Disease Classification Using Transfer Learning Approach

Sonia Verma[1], Ganesh Gopal Devarajan [1] and Pankaj Kumar Sharma [2]

[1] Department of Computer Science and Engineering, Faculty of Engineering and Technology, SRM Institute of Science and Technology, Delhi - NCR Campus, Delhi - Meerut Road, Modinagar, Ghaziabad, Uttar Pradesh 201204, India

[2] Department of Computer Science ABES Engineering College, Ghaziabad, UP, India

LINK	RECEIVED	ACCEPTED	PUBLISHED ONLINE	ASSIGNED TO AN ISSUE
https://doi.org/10.37575/b/eng/240032	29/07/2024	04/03/2025	04/03/2025	01/06/2025
NO. OF WORDS	**NO. OF PAGES**	**YEAR**	**VOLUME**	**ISSUE**
5703	8	2025	26	1

ABSTRACT

Chest X-ray (CXR) studies can be automatically detected, and their locations can be identified using artificial intelligence in healthcare. The World Health Organization reports that lung diseases such as COVID-19, pneumonia, tuberculosis, and lung opacity contribute significantly to global mortality. The overlapping symptoms of these diseases make accurate identification difficult. To accelerate the process and enable early detection, machine learning (ML) and traditional approaches are combined to improve disease detection. CXR images are used in this study to classify lung disease using ML and transfer learning (TL). The study primarily consists of three parts: firstly, the data augmentation technique addresses class imbalance; secondly, the image enhancement and pre-processing technique improves image quality; and finally, the TL approach EfficientNetB1 extracts features and uses weighted binary cross-entropy loss to handle a large number of false positive cases. Fine-tuning hyperparameters significantly enhance performance. AUC-PR, ROC-AUC, F1-score, and precision are among the metrics that demonstrate the proposed method to be more accurate and effective than other TL models.

KEYWORDS

Computer vision, COVID-19, deep learning, efficientNetB1, pneumonia, transfer learning

CITATION

Verma, S., Devarajan, G.G. and Sharma, P.K. (2025). Modified efficient net of chest x-ray images for lung disease classification using transfer learning approach. *Scientific Journal of King Faisal University: Basic and Applied Sciences*, **26**(1), 35–42. DOI: 10.37575/b/eng/240032

1. Introduction

Radiologists are instrumental in diagnosing and treating medical conditions by utilizing various imaging techniques, including computed tomography (CT) and positron emission tomography scans, magnetic resonance imaging, and chest X-ray (CXR). Nevertheless, using such a wide range of medical equipment presents challenges, the most difficult of which is interpreting chest radiographs (Cheng *et al.,* 2021). As modern industry and transportation have developed rapidly, air pollution has become a serious problem, leading to a significant increase in the prevalence of lung disease. Even highly qualified radiologists invariably commit 3%–6% of clinical errors in CXRs, and between 20% and 50% of reports are faulty (Wang *et al.,* 2019). According to a World Health Organization report, chronic obstructive pulmonary disease (COPD) is the third leading cause of death globally. Reports from various parts of the world have recently highlighted numerous cases of lung infections, including pneumonia, COVID-19, and lung opacity. Figure 1a shows the last three years' data of confirmed cases, while Figure 1b depicts the mortality rate of lung-affected COVID-19 patients (Mathieu *et al.*, 2020). Similar lung conditions, such as pneumonia, COVID-19, lung cancer, and lung opacity, are currently affecting several people worldwide. The healthcare sector has undergone a digital transformation that includes early diagnosis, virtual consultation, and remote access to reduce disease transmission (Kasinathan and Jayakumar, 2022). Due to the shortage of physicians and radiologists, the pandemic has brought about a new wave of complications in the healthcare sector, increasing the mortality rate of patients with chronic conditions, particularly those affected by cancer, diabetes, and heart disease.

Machine learning (ML) can be highly beneficial to healthcare informatics in terms of disease prognosis, classification, and screening. CT scans and CXR images are frequently used for lung disorders. CXRs provide a straightforward and affordable imaging method for grading and diagnosing lung conditions. The radiation exposure for a 2D projection image of the chest and lungs produced by X-rays is relatively low. Despite its limitations in 3D lung visualization, chest CT, which provides 3D imaging, is steadily gaining ground. Chest CTs are routinely used to identify lung nodules, although they expose individuals to more radiation than usual (Chowdhury *et al.,* 2020). However, in less developed countries, CXR continues to be the primary tool for diagnosing or screening tuberculosis. According to Tan *et al.,* (2018), radiologists can use these radiological imaging techniques in screening settings to identify lung problems or recommend additional testing. As a result, early lung disease identification and classification have become increasingly critical. ML and deep learning (DL) (Kumar, 2020) play an important role in handling and accelerating such processes.

This research aims to improve object detection in CXR for disease identification. The three models – YOLOv5, EfficientDet, and Faster R-convolutional neural network (CNN) – each contributed to the study in different ways. In Faster R-CNN (Ravi *et al.,* 2023), a ResNet50 backbone is used, along with a region proposal network (RPN) and classifier. RPNs generate region proposals, while classifiers utilize ResNet50 (Geddes, 2020) to classify objects based on predicted bounding box coordinates. Models with anchor boxes of varying sizes and aspect ratios can handle objects in various shapes and sizes. In YOLOv7 (Syed *et al.,* 2023), bounding boxes and class probabilities are predicted by considering one object at a time. This version allows users to choose between different network architectures, including CSPDarknet53 and CSPResNeXt50. For specific datasets, K-means clustering enhances the model's efficiency and accuracy by optimizing anchor box sizes (Li *et al.,* 2022) and aspect ratios.

1.1. Paper Contribution:

This paper makes the following substantial contributions:

1. Image enhancement and pre-processing are applied to enhance and standardize images.
2. A data augmentation technique is used to balance the dataset.

Corresponding Author: Sonia Verma 0091 8218634036, sonverma@gmail.com

However, this approach may reduce the number of generalization errors, particularly for classes with smaller sample sizes.
3. Feature extraction is performed using the transfer learning (TL) approach, EfficientNetB1, along with weighted binary cross-entropy loss to manage the high number of false positive cases.
4. The effectiveness of mEffCxrNet is evaluated in comparison to ResNet155v2, DenseNet-121, VGG-19, Mask R-CNN, bidirectional LSTM, MobileNetV2 with exponential fine-tuning, wavelet transformation, and EfficientNet, among others.

2. Literature Review

The lungs are among the most exposed organs in the body and have been a leading cause of death and disability for the past 200 years (Geddes, 2020). Developing a model that effectively analyses medical images is challenging because medical images are inherently more complex and heterogeneous than standard images. Numerous studies have explored the use of CXR images to identify various lung infections, including but not limited to pneumonia and COVID-19 (Ravi *et al.,* 2023).

TL and CNNs have proven effective in automatically extracting features from unstructured data, such as images, due to their advanced feature extraction capabilities. This research presents a comparative analysis of lung diseases in Table 1. The study focuses on a realistic dataset of patients with COPD (Hemdan *et al.,* 2020) to demonstrate the model's effectiveness in detecting COVID-19 and other lung diseases (Singh *et al.,* 2021).

Table 1. Literature summary and limitations

Author	Methodology	Features	Challenges
Syed *et al.,* (2023).	Optimised ResNet50v2	PF-positive individuals can be automatically classified using chest CT images based on the diagnostic model.	Did not conduct cross-validation experiments to confirm the reliability of the findings.
Li *et al.,* (2022)	Inception-ResNet v2	The prediction model combines Attention-U-Net and Inception-ResNet to improve the accuracy of CXR predictions.	Model complexity can be optimized due to insufficient computational training data.
Raza et al., (2023).	Inception-ResNet-v2	Achieves high classification accuracy.	The dataset is limited.
Yaseliani *et al.,* (2022).	VGG16 + VGG19	Displays improved performance metrics.	Requires fine-tuning.
Souid *et al.,* (2021).	MobileNet V2	Incorporates extra global average pooling and a dense layer.	AUC = 0.762 and F1-score = 0.652 are too low.
Cheng *et al.,* (2021).	DSAE	Effectively removes noise from the input signal.	Training is expensive due to complex data.
Hussain *et al.,* (2021)	CNN	The proposed method creates a sizable dataset to evaluate classification algorithms.	Model performance is low due to a limited number of images.
Ismael and Şengür (2021)	CNN	Achieves better classification accuracy using the kernel function.	Does not consider various lung diseases.
Karthik *et al.,* (2021).	CNN	Pneumonia classes can be optimally distinguished based on learning differentiating patterns.	Ineffective in learning definite patterns to assist radiologists in disease identification.
Cheng *et al.,* (2021).	BAT	Enhances local search capabilities and algorithm stability.	The dataset is small.
Bharati *et al.,* (2020).	ResNetv2	Uses ResNetv2 to categorise and locate abnormal regions.	Precision = 0.64, Recall = 0.62, and Accuracy = 70.8% – all relatively low.
Panwar *et al.,* (2020).	Grad-CAM	CXR images received a strong response.	Classification accuracy was not very high.
De Moura *et al.,* (2020).	DL	Provides reliable and rigorous analysis to assist clinical decision-making.	Deep learning is difficult and expensive in practice.
Arias-Londoño *et al.,* (2020).	DNN	Aims to improve specificity and classification accuracy.	Error distribution among classes remains an issue.
Rajaraman *et al.,* (2020).	CNN	Trimmed techniques precisely pinpoint the prominent ROI.	Requires an enormous amount of training data.

The literature review identified several gaps:

1. Effectively analyzing medical images is challenging due to limited data availability and their complexity.
2. Most TL methods overlook challenges such as improving X-ray image quality and handling class imbalance, which hinder the accurate identification of infected areas during feature extraction.
3. Existing approaches often extract features from complete lung images, disregarding the relevance of infected lung regions.
4. High training times pose significant challenges for CXR image classification and detection. The proposed model addresses this by achieving efficient classification on large datasets with reduced training time.

3. Methodology

The methodology aims to improve the accuracy and reliability of the CXR model by enhancing and standardizing images. Image enhancement and pre-processing techniques are applied to reduce noise and ensure uniformity across datasets. A data augmentation technique is used to address data imbalance by enlarging underrepresented classes and reducing overfitting risks. This approach minimizes generalization errors for smaller classes, ensuring balanced learning. Feature extraction is performed using the EfficientNetB1 TL model, which captures intricate patterns in medical images. A weighted binary cross-entropy loss function is integrated into the model to effectively manage the disproportionately high number of false positives that arise in medical diagnosis.

3.1. Pre-processing: Image Enhancement:

3.1.1. Standardisation

Standardizing an image involves subtracting its mean pixel value and dividing the result by its standard deviation. This process converts all images from the original grayscale into a standard grayscale, where similar intensities correspond to similar tissue characteristics, correcting inter-subject intensity variance (Hassan *et al.,* 2022).

Standardization normalizes a random variable by assigning it an expected mean value of 0 and a standard deviation of 1 (Dzierżak, 2019). The Z-test formula guides this procedure:

$$Z = \frac{x-\mu}{\sigma} \quad (1)$$

Based on Equation (1), the standardization formula calculates the value Z using the observed value x, the expected mean μ, and the standard deviation σ.

3.1.2. Class Imbalance

Class imbalance (Muljo *et al.,* 2023) occurs when a dataset contains a disproportionate number of examples from a single class, making it a prominent issue. This may appear as a classification problem with a distinct majority-minority class distinction or as a multiclass classification problem.

Table 2. Augmentation parameters for class balancing

Transformation	Techniques
Flip-horizontally	TRUE
Flip-vertically	TRUE
Rotational-range	20
Shift-width-range	0.2
Shift-height-range	0.2
Zoom-range	0.2
Shear transformation	20

Due to imbalance, the model skews toward predictions for the majority class, making imbalanced datasets problematic. Accuracy also becomes a misleading performance metric in such cases. A data augmentation technique is employed to balance the class distribution. A dataset containing an uneven ratio of samples between the majority and minority classes is referred to as class imbalance.

Shear transformation is a method that fixes one axis of an image while stretching the other at a predetermined angle, for example, a 0.2 shear angle. Random zoom transformation was performed using the zoom range argument; a value greater than one indicates that the images were zoomed in, while a value less than one indicates that they were zoomed out. To balance the dataset, augmented images were created for minority classes based on the maximum size of the majority class. Out of four classes, the majority class, 'Normal,' has 7,146 samples; thus, the other minority classes were sampled to match this number. The augmentation process increased the number

of images by 13,737, bringing the total training dataset size to 28,584. Table 2 presents the data augmentation transformation techniques applied to balance the data.

3.1.3. EfficientNet Model

The EfficientNetB1 method was introduced by Google AI (Raza *et al.,* 2023) to solve the problem of accurate prediction using an efficient approach. The EfficientNet algorithm was initially developed by Tan and Le in 2019. This TL algorithm performs well on both common and ImageNet image classification tasks.

To classify lung diseases from CXR images, we fine-tuned the EfficientNetB1 architecture. Figure 1 depicts the model architecture of mEffCxrNet. Optimizing the network's depth, width, and resolution can improve performance by scaling the network model.

Figure 1. Architecture of model

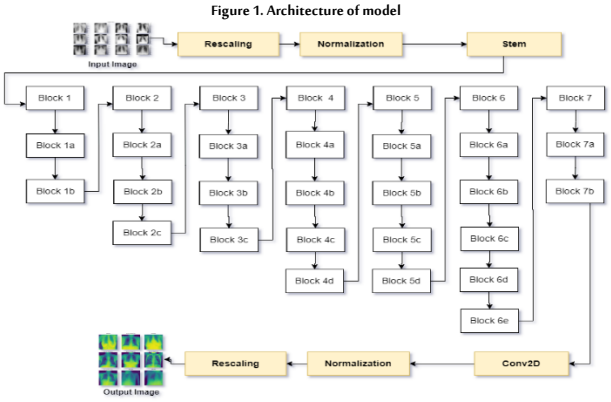

It can enhance local search capabilities and guarantee algorithm stability. It achieves excellent accuracy and performs better than other methods with a huge amount of data. The CXR images receive a strong response; COVID-19 cases are not identified in the present scenario, and the cropped techniques precisely identify the prominent ROI. The amount of data needed for training is enormous.

In order to scale EfficientNet (Tan and Le, 2020) in three aspects — width (w), depth (d), and resolution (r) — it includes a fixed set of scaling coefficients that follow predefined guidelines. For n output classes, the likelihood distribution is computed using the SoftMax function, given in Equation (2). Here, x, y, and z are constants computed through a hyperparameter tuning process known as grid search, where φ is user-specified and manages computational resources accordingly.

$$d = x^{\varphi}$$
$$w = y^{\varphi}$$
$$r = z^{\varphi}$$
$$s.t\ \alpha.\beta^2.\gamma^2 \approx 2$$
$$\alpha \geq 1, \beta \geq 1, \gamma \geq 1 \quad (2)$$

Scaling coefficients were applied to the baseline network to achieve the desired target model size. The accuracy of images increases marginally as the image width or resolution increases. To solve this problem, it is important to adjust all these dimensions simultaneously.

It is possible to express the CNN using the following expression:

$$O_i = f_i$$

Where f_i represents the operator, t_o represents the output image and X_i represents the input image. The input CXR image X_i has the shape (H_i, W_i, C_i), where spatial dimensions are H_i, W_i, and the channel dimension is C_i so the ConvNet of the EfficientNet-B1 model is represented as a series of layers: $L = f_k \ldots \ldots \ldots \ldots f_1(X_i)$ and finally, ConvNet is represented as:

$$N = \bigcirc_{i=1}^{s} f_{Li}(X_{H_i,W_i,C_i}) \quad (3)$$

Here, the shape of the input image X_i is represented by H_i, W_i, C_i, and f_{Li} *represents* f_i applied l_i times in stage i. To optimize the outcome, it is important to scale the model by adjusting the network length (L_i), and with shape H_i, W_i.

$$s.t.\ N(d, w, r) = \bigcirc_{i=1}^{s} f_{d.Li}(X_{r.H_i, r.W_i, w.C_i}) \quad (4)$$

In Equation (4), N illustrates the network with predefined baseline model parameters F_i, L_i, H_i, W_i, C_i, where i is the stage number. These parameters are scaled with width, resolution, and depth d, r, w. EfficientNet-B1 has 344 layers with three color channels (R, G, and B), with each input image having a size of 400 × 400 pixels. The resolution of subsequent layers is scaled down to reduce the feature map size while the width is increased for accuracy. For instance, the second convolution (CNN) layer consists of W = 16 filters, and the following convolution layer has W filters. For example, Conv2D has W = 16 filters, while the third CNN layer has W = 24 filters. The final layer, which is fed to the fully connected layer, has an upper limit of D = 1469 filters.

By combining Plateau, Early Stopping, and Model Checkpoint Keras callbacks, the model effectively addresses some of their drawbacks.

Algorithm: Pseudo-Code for mEffCxrNet

Input: Covid19-Radiography-Database

Output: A model for lung disease classification

```
Begin
1   data ← load dataset
2   check_ims_in_folder ← data
3   Check_label_distribution ← x
4   Found:
5       Class_imabalace ← dataset(positive sample>>negative sample)
        b_x ← balance dat (data_augmentation)
6       Add: train_ ata(x) and test_dat (y)
7   x,y ← spli (x1,x2,y1,y2)
8   Standardization ← Z = (x − μ)/σ
9   img_gen:
        img_size = (300,300,1)
        b_size = 64
        t_size = (300,300)
10  img_merge ← x,y
    img_split ← x,y
11  L_cross_entropy ← cross_w − loss_entropy
12      Restore_be t_weight = True
13      classifier ← train_model using b_x
        model.fit ← EfficientNetB1(mEffCxrNet)+additional layer
            Activation ← Softmax, relu
            k_r ← l2(l = 0.016)
            a_r ← l1(0.006)
            b_r ← l1(0.006)
            momentum ← 0.99
            optimizer ← Adamax
14      Predict ← cross_validation with model
        computes evaluation_metrics
End
```

Early stopping based on user-specified accuracy criteria and dynamic learning rate modifications is possible due to the weighted cross-entropy loss. The cross-entropy loss contribution from the i^{th} training dataset is computed as follows for each CXR image in this study:

$$L_{cross\_entropy(x_i)} = -(\ y_i\ \log(f(x_i)) + (1 - y_i\ )\log(1 - f(x_i))) \quad (5)$$

Where $f(x_i)$ represents the model output or the likelihood of a

correct classification while (x_i) and (y_i) denote the input characteristics and corresponding label, respectively. In each training scenario, where $(y_i) = 0\ or\ (1 - y_i) = 0$, only one of these terms contributes to the loss (as the other term is divided by zero and becomes equal to zero).

The average cross-entropy loss across a training set of N instances, denoted as D, can be expressed in the following manner:

$$L_{cross\_entropy} = -\frac{1}{N}\left(\sum_{n_{pos}} \log\left(f(x_i)\right) + \sum_{n_{neg}} \log\left(1 - f(x_i)\right)\right) \quad (6)$$

In scenarios where positive training instances are significantly fewer, the negative class dominates the loss. Whether each class contributes positively or negatively is determined based on its total contribution across all training cases related to the pathological condition:

$$freq_p = \frac{n_{pos}}{w_{pos}}, \text{and} \quad freq_n = \frac{n_{neg}}{w_{neg}} \quad (7)$$

Where n_{pos} and n_{neg} represent the number of positive and negative examples, respectively. To equalize the overall contribution of each class, each instance is multiplied by the class-specific weight factors w_{pos} and w_{neg}. The desired balancing condition is:

$$w_{pos} * freq_p = w_{neg} * freq_n \quad (8)$$

which we can achieve simply by applying the weightings. The positive and negative labels within each class would have the same overall contribution to the loss function, as seen in the above image if these weightings were applied. Now, let us implement such a loss function. The final weighted loss for each training case after calculating the weights is:

$$L_{cross\_entropy(x_i)} = -\left(w_{pos} y \log\left(f(x)\right) + w_{neg}(1 - y)\log(1 - f(x))\right) \quad (9)$$

By reducing the weighted cross-entropy loss, the model becomes less biased towards the majority class and improves its ability to classify all classes accurately, particularly those underrepresented in the dataset.

4. Results

4.1. Dataset Description:

Evaluation of the proposed framework is conducted using publicly available Kaggle Mathieu *et al.*, (2020) that is, the COVID-19 Radiography Dataset (Nguyen *et al.*, 2020). The dataset contains 21,212 images. Upon the initial release, our database contained 219 CXR images of COVID-19, along with 1,341 CXR images of standard pneumonia and 1,345 CXR images of viral pneumonia.

Figure 2: A visualization of the dataset's class distribution and description

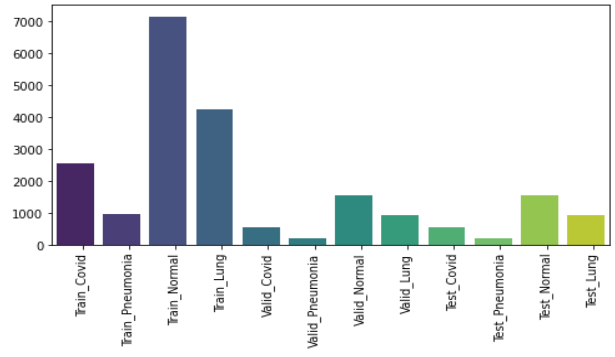

Figure 2 illustrates the basic distribution of the proposed dataset, which combines data sources into a single dataset repository containing raw CXR image data from a lung-infected patient. Each folder was checked for available data and label distributions. After the distribution, it was noticed that the positive samples were significantly more significant than the negative samples, indicating an imbalance in the class.

Therefore, we applied class balancing and measured the intensity distribution of pixels before and after standardization for image enhancement. To build the model, an augmentation layer, a pre-processing layer, and a custom lambda layer were added using EfficientNetB1 with the pre-trained image. We use weighted binary cross-entropy loss to handle false positives, aiming to achieve the best result.

Since there are many more X-ray images of pneumonia, the model weighs these cases heavily, leading to incorrect classifications. Thus, we adjust this bias and attempt to force the model to balance normal and pneumonia images. The performance metrics evaluate the model's effectiveness.

4.2. Performance Measures:

The hardware and software environment used in the experiment are as follows: Windows 10 Pro edition with a 64-bit operating system, x64-based processor, Intel(R) Core(TM) i5-8250U CPU @ 1.60GHz–1.80GHz, 8 GB memory, and GPU100 with 16 GB memory. Python was used as the primary programming language to execute the work.

Performance metrics, including accuracy, specificity, recall, precision, false positive rate (FPR), false negative rate (FNR), and F1-score, were calculated to assess the TL models. Each unique model's confusion matrix was used to derive these parameters. The most commonly used metrics in image annotation were employed to evaluate the effectiveness of the proposed model, including:

Accuracy: Accuracy is a metric used to evaluate the effectiveness of classification and regression methods. It is defined as the ratio of correct predictions to the total number of predictions:

$$Accuracy = \frac{t_p + t_n}{t_p + t_n + f_p + f_n} \quad (10)$$

Here, t_p, t_n, f_p and f_n represent true positives, true negatives, false positives, and false negatives, respectively.

Precision (p): Based on the number of predicted values that are actually correct, precision indicates the proportion of accurately made positive predictions. It is calculated as follows:

$$p = \frac{t_p}{t_p + f_p} \quad (11)$$

Recall(r): Recall measures the proportion of correct positive predictions among all actual positive cases:

$$r = \frac{t_p}{t_p + f_n} \quad (12)$$

$F1 - score$: F1-score is a metric used to evaluate binary classification models based on the predictions made for the positive class. It is calculated by combining precision and recall while assigning equal weight to both. The formula is:

$$F1 - score = \frac{2 * t_p}{2 * t_p + f_p + f_n} \quad (13)$$

Specificity (S_p): Specificity measures the percentage of patients correctly identified as normal (having no lung disease). Patients with any lung disease, such as lung opacity, are categorized as TN and FP – those who are actually not suffering from lung opacity. This metric determines which lung disease belongs to which class:

$$S_p = \frac{t_n}{t_n + f_p} \quad (14)$$

Table 3 presents the performance measures and their values, demonstrating the effectiveness of the proposed model.

Table 3. Performance measures

Measure	Value(%)
Precision	99.44
Recall	99.26
Sensitivity	99.26
Specificity	99.89
Positive Predictive Value (Precision)	99.45
Negative Predictive Value	99.85
False Positive Rate	0.11
False Discovery Rate	0.55
False Negative Rate	0.74
Accuracy	99.78
F1 Score	99.35
Matthews Correlation Coefficient	99.22

Matthews Correlation Coefficient (MCC): According to the confusion matrix, MCC yields a high score only if the model performs well in all four categories (TP, TN, FP, FN), maintaining a balance between the size of positive and negative variables in the dataset:

$$\frac{t_p * t_n - f_p * f_n}{\sqrt{(t_p+f_p)*(t_p+f_n)*(t_n+f_p)*(t_n+f_n)}} \quad (15)$$

4.3. Result Analysis

An Adamax optimizer was used for learning rate optimization over 20 epochs with 75% training data, 15% validation data, and 15% testing data. The Adamax optimizer significantly enhanced model performance, and fine-tuning with optimized learning rates further improved accuracy.

Figure 3. Training and validation curve

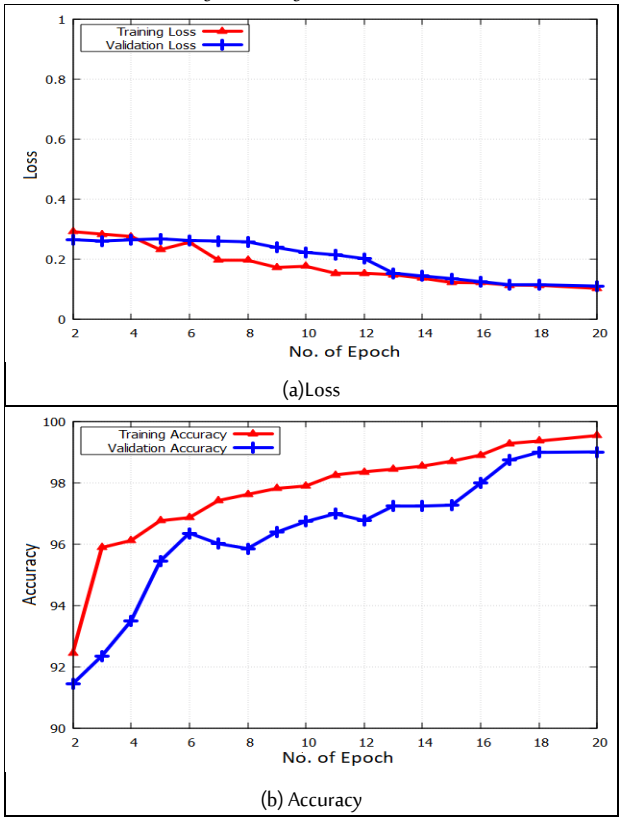

(a)Loss

(b) Accuracy

Figure 4. Precision and recall curve

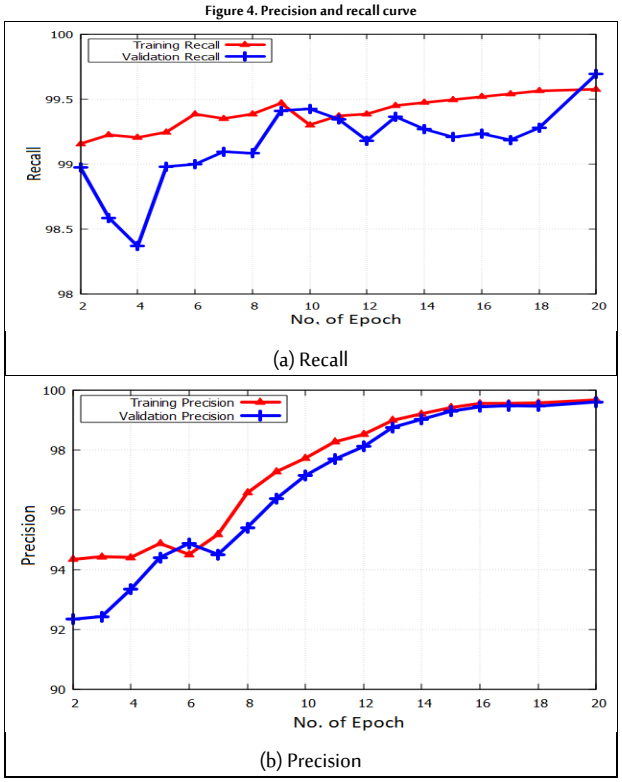

(a) Recall

(b) Precision

Figure 5: Performance Measure Graph

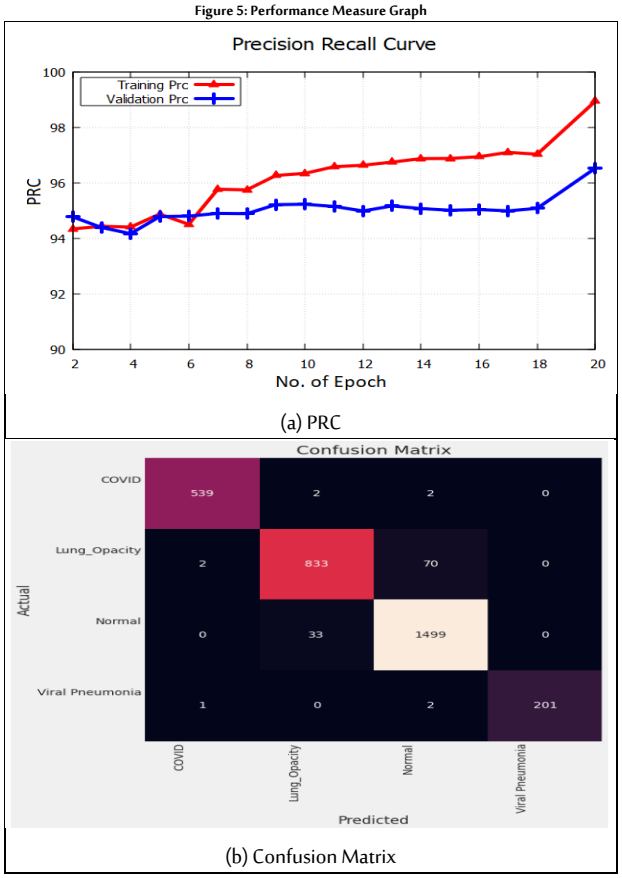

(a) PRC

(b) Confusion Matrix

Figure 3(a–b) shows the loss and accuracy values during the validation and training phases of the proposed model. In Figure 5(a–b), the y-axis represents loss/accuracy, and the x-axis represents the number of epochs. Figure 4(a–b) shows Precision and Recall values on the y-axis with a number of epocs on the x-axis. Figure 5(a)

represents the proportion of true positive predictions among all positive predictions made, while Figure 5(b) shows the ratio of true positive predictions to the total number of actual positive cases. The classification decisions were analyzed using confusion matrices and contingency tables. Additionally, the ROC curves in Figure 6(a) illustrate the decision-making process in diagnostic tests, where the ROC graph shows the relationship between the true positive rate (Sensitivity, Y-axis) and the false positive rate (Specificity, X-axis).

4.4. Comparative Analysis:

Based on the experiment results, it can be concluded that the proposed model offers substantial improvements in terms of accuracy, speed, and cost for lung disease classification using CXR images. The suggested model outperforms other models in statistical metrics, as shown in Table 4, leading to improved generalization, better accuracy, and fewer incorrect predictions.

Table 4. Comparison with state-of-the-art methods

Reference	Method	Accuracy	Precision	Recall	F1-Score	Chest X-ray images
Chakraborty *et al.*, (2022)	VGG-19	97.11	97	97	96	3,797
Fernando *et al.*, (2022)	ResNet152V2	98.96	97.52	98.64	98.25	5,386
Kaur and Kulkarni (2024)	MobileNetV2 + Exponential Fine-Tuning	96.89	96.72	96.71	96.9	9,475
Indumathi and Siva (2023).	Mask R-CNN + Bidirectional LSTM	99.16	99.18	99.16	99.14	13,808
Al-Ahmadi and Mohammad (2023)	Wavelet Transformation and EfficientNet	97	96	89	92	5,544
Showkat and Qureshi (2022).	ResNet Model	95	95.65	94	95	1,428
Our Model		99.39	98.89	97	97	21212

Figure 6(b) shows a comparative analysis of the proposed model with other models such as VGG-19, ResNet50, MobileNetV2 + Exponential Fine-Tuning, Deep CNN + ResNet50, Mask R-CNN + Bidirectional LSTM, Wavelet Transformation and EfficientNet, ResNet Model, CoviXNet, and Wide ResNet50. The analysis shows that mEffCxrNet performed better in terms of accuracy and speed.

Figure 6. Decision-making measures

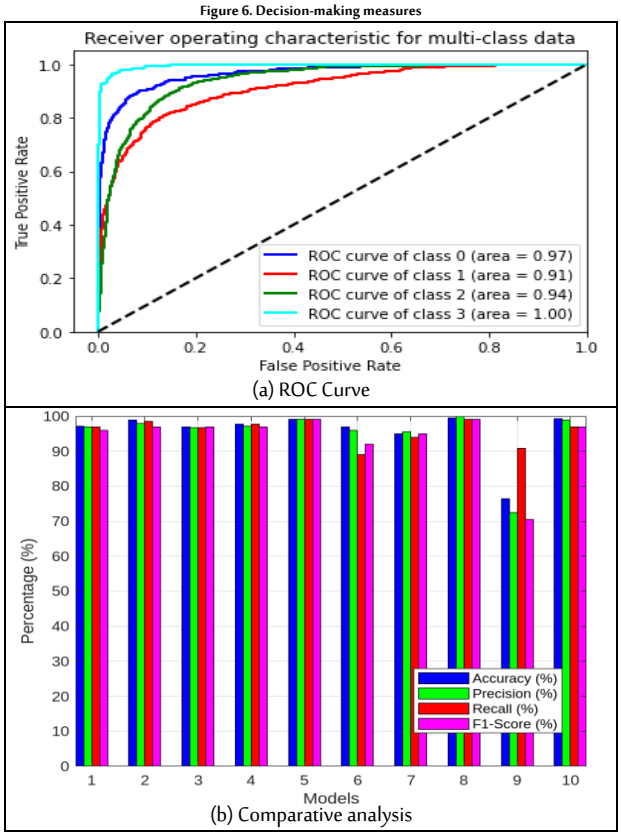

(a) ROC Curve

(b) Comparative analysis

5. Conclusion and Future Work

We can use a categorization system to compare CXR images of COVID-19 patients and those with normal pneumonia. COVID-19 significantly disrupts daily life, affecting everything from public healthcare to the global economy. This work introduced the mEffCxrNet model, which employs CXR to classify positive lung disease. The proposed model, mEffCxrNet, successfully provides precise diagnoses for four class divisions: COVID-19, lung opacity, viral pneumonia, and normal. To the best of our knowledge, the suggested framework achieves the highest accuracy on the datasets used in the experiments, with a classification accuracy of 99.70%, precision of 98.68%, recall of 98.67%, F1-score of 98.67%, and the lowest error rate of 1.33%. It consists of multiple layers, including an input layer, the primary capsule, and the first convolutional layer. Moreover, models can be retrained and reused, and image analysis can help identify further abnormalities. In this research, the use of CXR images – a practical, effective, and affordable testing method – has been investigated for the quick and accurate identification of COVID-19 in patients. Using our dataset, we experimented with and examined many pre-trained models. On the top-performing models, we also performed a 4-class classification. Future versions of this method may be implemented as a real-time CT scan by integrating high-end GPUs, cloud computing, patient data security, and appropriate software interfaces.

Biographies

Sonia Verma

Department of Computer Science and Engineering, Faculty of Engineering and Technology, SRM Institute of Science and Technology, Delhi - NCR Campus, Delhi - Meerut Road, Modinagar, Ghaziabad, Uttar Pradesh 201204, India, 0091 8218634036, sonverma@gmail.com

Sonia, an Indian researcher, holds M.Tech. in Computer Science and Engineering and is currently pursuing a Ph.D. With over 10 years of experience in academia and industry, she serves as an Assistant Professor at ABES Engineering College, Ghaziabad (U.P.). She is a reviewer for SCI-indexed journals, with research interests in Machine Learning, Artificial Intelligence, IoT, and Cloud Computing. She has published extensively in reputed SCI/Scopus-indexed journals and conferences.

ORCID: 0000-0002-2384-472X

Ganesh Gopal Devarajan

Department of Computer Science and Engineering, Faculty of Engineering and Technology, SRM Institute of Science and Technology, Delhi - NCR Campus, Delhi - Meerut Road, Modinagar, Ghaziabad, Uttar Pradesh 201204, India,

0091 9444540447, dganeshgopal@gmail.com

Prof. Ganesh (Member, IEEE) received his Ph.D. in Computer Science and Engineering from VIT University, Vellore, in 2015. With over 17 years of research and teaching experience, he is a Professor at the School of Computing Science and Engineering, SRM Institute of Science and Technology, Chennai. He has served as a Technical Program Committee member, Program Committee member, and Session Chair at prestigious international conferences and is a member of professional bodies such as ACM and CSI.

ORCID: 0000-0003-0036-7841

Pankaj Kumar Sharma

Department of Computer Science, ABES Engineering College, Ghaziabad, India, 00919899346360, pankaj.sharma@abes.ac.in

Prof. Pankaj is a distinguished scholar in Computer Science with over 18 years of experience in academia and industry. He holds a Ph.D. and an M.Tech. in Computer Science and has made significant contributions to System Modeling & Simulation, Artificial

Intelligence, Machine Learning, Data Analytics, and Wireless Mobile Ad Hoc Networks. His research expertise spans multiple cutting-edge domains, reflecting his dedication to advancing technological innovation and academic excellence.

ORCID: 0000-0003-2793-6100

Data Availability Statement

The data that support the findings of this study are available on request from the corresponding author.

Acknowledgments

The authors extend their appreciation for the continued support of SRM University.

Funding

This research received no external funding.

Conflicts of Interest

No conflicts of interest exist.

References

Al-Ahmadi, S. and Mohammad, F. (2023). Pattern recognition of omicron variants from amalgamated multi-focus EEG signals and X-ray images using deep transfer learning. *Egyptian Informatics Journal,* **24**(1), 129–38. DOI: 10.1016/j.eij.2023.01.001

Arias-Londono, J.D., Gomez-Garcia, J.A., Moro-Velazquez, L. and Godino-Llorente, J.I. (2020). Artificial intelligence applied to chest X-ray images for the automatic detection of COVID-19. A thoughtful evaluation approach. *Ieee Access*, **8**(n/a), 226811–27. DOI: 10.1109/ACCESS.2020.3044858

Bharati, S., Podder, P. and Mondal, M.R.H. (2020). Hybrid deep learning for detecting lung diseases from X-ray images. *Informatics in Medicine Unlocked*, **20**(n/a), 100391. DOI: 10.1016/j.imu.2020.100391

Chakraborty, S., Paul, S. and Hasan, K.A. (2022). A transfer learning-based approach with deep cnn for covid-19-and pneumonia-affected chest x-ray image classification. *SN Computer Science*, **3**(n/a), 1–10. DOI: 10.1007/s42979-021-00881-5

Cheng, J., Zhao, W., Liu, J., Xie, X., Wu, S., Liu, L. and Liu, J. (2021). Automated diagnosis of COVID-19 using deep supervised autoencoder with multi-view features from CT images. *IEEE/ACM Transactions on Computational Biology and Bioinformatics*, **19**(5), 2723–36. DOI: 10.1109/TCBB.2021.3102584

Chowdhury, M.E., Rahman, T., Khandakar, A., Mazhar, R., Kadir, M.A., Mahbub, Z.B. and Islam, M.T. (2020). Can AI help in screening viral and COVID-19 pneumonia?. *Ieee Access*, **8**(n/a), 132665–76. DOI**:** 10.1109/ACCESS.2020.3010287

De Moura, J., García, L.R., Vidal, P.F.L., Cruz, M., López, L.A., Lopez, E.C. and Ortega, M. (2020). Deep convolutional approaches for the analysis of covid-19 using chest x-ray images from portable devices. *Ieee Access*, **8**(n/a), 195594–1607. DOI: 10.1109/ACCESS.2020.3033762

Dzierżak, R. (2019). Comparison of the influence of standardization and normalization of data on the effectiveness of spongy tissue texture classification. *Informatyka, Automatyka, Pomiary W Gospodarce I Ochronie Środowiska*, **9**(3), 66–9. DOI: 10.35784/iapgos.62

Fernando, C., Kolonne, S., Kumarasinghe, H. and Meedeniya, D. (2022). Chest radiographs classification using multi-model deep learning: A comparative study. In: *2nd International Conference on Advanced Research in Computing (ICARC)*. Belihuloya, Sri Lanka, 23-24 /02/2022. DOI**:** 10.1109/ICARC54489.2022.9753811

Geddes, D. (2020). The history of respiratory disease management. *Medicine*, **48**(4), 239–43. DOI: 10.1016/j.mpmed.2020.01.007

Hassan, M., Shaikh, M.S. and Jatoi, M.A. (2022). Image quality measurement-based comparative analysis of illumination compensation methods for face image normalization. *Multimedia Systems*, **28**(2), 511–20. DOI: 10.1007/s00530-021-00853-y

Hemdan, E.E.D., Shouman, M.A. and Karar, M.E. (2020). Covidx-net: A framework of deep learning classifiers to diagnose covid-19 in x-ray images. *arXiv preprint arXiv:2003.11055*, **n/a**(n/a), n/a. DOI: 10.48550/arXiv.2003.11055

Hussain, E., Hasan, M., Rahman, M.A., Lee, I., Tamanna, T. and Parvez, M.Z. (2021). CoroDet: A deep learning based classification for COVID-19 detection using chest X-ray images. *Chaos, Solitons and Fractals*, **142**(n/a), 110495. DOI: 10.1016/j.chaos.2020.110495

Indumathi, V. and Siva, R. (2023). An efficient lung disease classification from X-ray images using hybrid Mask-RCNN and BiDLSTM. *Biomedical Signal Processing and Control*, **81**(n/a), 104340. DOI:10.1016/j.bspc.2022.104340

Ismael, A.M. and Şengür, A. (2021). Deep learning approaches for COVID-19 detection based on chest X-ray images. *Expert Systems with Applications*, **164**(n/a), 114054. DOI: 10.1016/j.eswa.2020.114054

Karthik, R., Menaka, R. and Hariharan, M.J.A.S.C. (2021). Learning distinctive filters for COVID-19 detection from chest X-ray using shuffled residual CNN. *Applied Soft Computing*, **99**(n/a), 106744. DOI: 10.1016/j.asoc.2020.106744

Kasinathan, G. and Jayakumar, S. (2022). Cloud-Based Lung Tumor Detection and Stage Classification Using Deep Learning Techniques. *Biomed research international*, **2022**(1), 4185835. DOI: 10.1155/2022/4185835

Kaur, S. and Kulkarni, N. (2024). FERFM: An enhanced facial emotion recognition system using fine-tuned mobilenetv2 architecture. *IETE journal of research*, **70**(4), 3723–37. DOI:10.1080/03772063.2023.2202158

Kumar, D. (2020). Feature extraction and selection of kidney ultrasound images using GLCM and PCA. *Procedia Computer Science*, **167**(n/a), 1722–31. DOI: 10.1016/j.procs.2020.03.382

Li, D., Liu, Z., Luo, L., Tian, S. and Zhao, J. (2022). Prediction of Pulmonary Fibrosis Based on X-Rays by Deep Neural Network. *Journal of Healthcare Engineering*, **2022**(1), 3845008. DOI: 10.1155/2022/3845008

Mathieu, E., Ritchie, H., Rodés-Guirao, L., Appel, C., Gavrilov, D., Giattino, C. and Roser, M. (2020). *Coronavirus (COVID-19) Cases*. Available at: https://ourworldindata.org/covid-cases (acssesd on 13/02/2025)

Muljo, H.H., Pardamean, B., Elwirehardja, G.N., Hidayat, A.A., Sudigyo, D., Rahutomo, R. and Cenggoro, T.W. (2023). Handling severe data imbalance in chest X-Ray image classification with transfer learning using SwAV self-supervised pre-training. *Commun. Math. Biol. Neurosci.*, **2023**(n/a), n/a. DOI: 1028919/cmbn/7526

Nguyen, H., Pham, H.H., Nguyen, N.T., Nguyen, D.B., Dao, M., Vu, V. and Le, L.T. (2020). *Vinbigdata Chest X-Ray Abnormalities Detection*. Available at: https://www. kaggle. com/c/vinbi gdatachest-xray-abnor malit ies-detec tion (acssesd on 13/02/2025)

Panwar, H., Gupta, P.K., Siddiqui, M.K., Morales-Menendez, R., Bhardwaj, P. and Singh, V. (2020). A deep learning and grad-CAM based color visualization approach for fast detection of COVID-19 cases using chest X-ray and CT-Scan images. *Chaos, Solitons and Fractals*, **140**(n/a), 110190. DOI: 10.1016/j.chaos.2020.110190

Rajaraman, S., Siegelman, J., Alderson, P.O., Folio, L.S., Folio, L.R. and Antani, S.K. (2020). Iteratively pruned deep learning ensembles for COVID-19 detection in chest X-rays. *Ieee Access*, **8**(n/a), 115041–115050. DOI: 10.1109/access.2020.3003810

Ravi, V., Acharya, V. and Alazab, M. (2023). A multichannel EfficientNet deep learning-based stacking ensemble approach for lung disease detection using chest X-ray images. Cluster Computing, 26(2), 1181–1203. DOI: 10.1007/s10586-022-03664-6

Raza, R., Zulfiqar, F., Khan, M.O., Arif, M., Alvi, A., Iftikhar, M.A. and Alam, T. (2023). Lung-EffNet: Lung cancer classification using EfficientNet from CT-scan images. *Engineering Applications of Artificial Intelligence*, **126**(n/a), 106902. DOI:10.1016/j.engappai.2023.106902

Showkat, S. and Qureshi, S. (2022). Efficacy of Transfer Learning-based ResNet models in Chest X-ray image classification for detecting COVID-19 Pneumonia. *Chemometrics and Intelligent Laboratory Systems*, **224**(n/a),104534. DOI: 10.1016/j.chemolab.2022.104534

Singh, R.K., Pandey, R. and Babu, R.N. (2021). COVIDScreen: explainable deep learning framework for differential diagnosis of COVID-19 using chest X-rays. *Neural Computing and Applications*, **33**(n/a), 8871–92. DOI: 10.1007/s00521-020-05636-6

Souid, A., Sakli, N. and Sakli, H. (2021). Classification and predictions of lung diseases from chest x-rays using mobilenet v2. *Applied Sciences*, **11**(6), 2751. DOI: 10.3390/app11062751

Syed, A.H., Khan, T. and Khan, S.A. (2023). Deep transfer learning techniques-based automated classification and detection of

pulmonary fibrosis from chest CT images. *Processes*, **11**(2), 443. DOI: 10.3390/pr11020443

Tan, M. and Le, Q. (2019). Efficientnet: Rethinking model scaling for convolutional neural networks. In: The 36th *International conference on machine learning*. PMLR. Long Beach, CA, USA, 10-15/06/2019.

Tan, T., Li, Z., Liu, H., Zanjani, F.G., Ouyang, Q., Tang, Y. and Li, Q. (2018). Optimize transfer learning for lung diseases in bronchoscopy using a new concept: sequential fine-tuning. *IEEE Journal of Translational Engineering in Health and Medicine*, **6**(n/a), 1–8. DOI: 10.1109/JTEHM.2018.2865787

Wang, C., Chen, D., Hao, L., Liu, X., Zeng, Y., Chen, J. and Zhang, G. (2019). Pulmonary image classification based on inception-v3 transfer learning model. *IEEE Access*, **7**(n/a), 146533–141. DOI**:** 10.1109/ACCESS.2019.2946000

Yaseliani, M., Hamadani, A.Z., Maghsoodi, A.I. and Mosavi, A. (2022). Pneumonia detection proposing a hybrid deep convolutional neural network based on two parallel visual geometry group architectures and machine learning classifiers. *IEEE access*, **10**(n/a), 62110–28. DOI**:** 10.1109/ACCESS.2022.3182498